Proceedings Paper:
Hosseinabadi, P.A., Negnevitsky, M., Siddique, M.D. et al. (2026) PSO-tuned fixed-time sliding mode voltage and current controllers for grid-forming inverters. In: 2025 IEEE International Conference on Energy Technologies for Future Grids (ETFG). 2025 IEEE International Conference on Energy Technologies for Future Grids (ETFG), 07-11 Dec 2025, Wollongong, Australia. Institute of Electrical and Electronics Engineers (IEEE). ISBN: 9798331576417.

https://doi.org/10.1109/ETFG61999.2025.11401144

2025 IEEE International Conference on Energy Technologies for Future Grids
Wollongong, Australia, December 7-11, 2025

PSO-Tuned Fixed-Time Sliding Mode Voltage and Current Controllers for Grid-Forming Inverters

1st Pooyan Alinaghi Hosseinabadi
School of Engineering
University of Tasmania
Hobart, Australia
https://orcid.org/0000-0002-9061-086X

2nd Michael Negnevitsky
School of Engineering
University of Tasmania
Hobart, Australia
https://orcid.org/0000-0002-5130-419X

3rd Marif Daula Siddique
School of Engineering
Swinburne University of Technology
Melbourne, Australia
https://orcid.org/0000-0002-0799-500X

4th Saad Mekhilef
School of Engineering
Swinburne University of Technology
Melbourne, Australia
https://orcid.org/0000-0001-8544-8995

5th Hemanshu Pota
Department of Electrical Engineering
The University of New South Wales
Canberra, Australia
https://orcid.org/0000-0002-9612-714X

6th John Anthony Rossiter
School of Electrical and Electronic Eng
The University of Sheffield
Sheffield, United Kingdom
https://orcid.org/0000-0002-1336-0633

***Abstract*—This paper focuses on enhancing the performance of capacitor voltage and inverter current controllers for grid-forming inverters (GFMIs) equipped with an LC filter, ensuring seamless transitions from off-grid to grid-tied modes. A novel Particle Swarm Optimization-Tuned Fixed-time Sliding Mode Control (PSO-FSMC) method is introduced and applied within a cascaded voltage and current control framework for GFMIs. This paper presents a new and straightforward approach for designing sliding surfaces and control laws of the FSMC, specifically focusing on balancing chattering reduction, singularity avoidance, and ensuring both rapid response and strong robustness. An innovative application of the PSO algorithm optimizes 24 control parameters of the FSMC, aimed at reducing tracking errors during transitions from off-grid to on-grid modes. The effectiveness of the proposed PSO-FSMC is rigorously tested and compared with well-established PI voltage and current controllers through simulations conducted in MATLAB/SimPowerSystems. The behavior of the closed-loop system using the proposed controller is evaluated during transitions from autonomous to grid-connected modes under both ultra-weak and ultra-strong grid conditions. Results confirm that the proposed method significantly outperforms the PI controller, achieving a 97% reduction in tracking errors in both transient and steady-state responses.**

***Index Terms*—SMC, GFMI, robustness, PSO, fixed-time.**

I. Introduction

THE operation of power grids is transitioning from traditional synchronous machines (SMs) to a more dominant role for inverter-based resources (IBRs). The inverters used in IBRs are generally designed to follow grid voltages and inject current into the existing voltage, hence they are known as grid-following inverters (GFLIs). A key component in their synchronization with the grid is the phase-locked loop (PLL), which can negatively impact the stability of voltage source inverters under weak grid conditions [1]. Furthermore, unlike SMs, the rapid expansion of IBRs based on GFLIs introduces significant challenges due to their inherently low inertia, which causes them to respond quickly to stochastic events, potentially leading to stability and robustness issues [2]. In response, there is an increasing shift towards adopting grid-forming inverters (GFMIs). Distinct from grid-following inverters, GFMIs act as both voltage and frequency regulators without the need for a PLL. This capability not only enhances the power grid's stability and robustness by simulating inertia, but also provides crucial support during power outages, enabling it to act as the primary power source in black start events [3]. However, effective control of GFLIs is crucial to ensure a seamless transition for IBRs from off-grid to grid-tied mode, especially within the voltage and current control loops.

The control architecture of GFLIs typically incorporates multiple nested loops, including voltage and current control loops, as well as power synchronization control loops (primary layer). In the primary layer, droop control is widely used for power synchronization, due to its simplicity and effectiveness [1]. Focusing on cascaded voltage and current control loops, the most commonly adopted controllers are proportional-integral (PI) controllers [1]. Although PI controllers are favored for their simple structure and ease of implementation, tuning the parameters of cascaded PI controllers is challenging and heavily dependent on a precise model of the GFMI system to achieve the desired performance. Furthermore, PI controllers are sensitive to stochastic events during operation, such as transitions from off-grid to grid-connected modes, which can degrade their performance, highlighting the need for further improvements.

Numerous control techniques have been employed for cascaded loop control in inverters, including table-based control [4], predictive control [5], and repetitive control [6]. Each of these methods, however, has its own set of limitations: table-based and intelligent control may generate undesirable current harmonics due to variable switching frequencies, predictive control requires precise system parameters for optimal perfor-

mance, and repetitive control is confined to static conditions with slow response times.

A high-order sliding mode control (SMC) for GDMIs has been proposed in [7] and compared with conventional vector control, which includes PI controllers. Although the results show improved response time and enhanced robustness to stochastic events, the proposed method employs a single-loop voltage controller, which may compromise safety in real-world implementations due to the potential for current to exceed safe limits. Furthermore, an asymptotic SMC-based inner current controller is introduced in [8] to deliver fast and robust performance within the inner current loop. Despite these advancements, the SMC has not been incorporated into the outer voltage controller, and no solution has been presented to address the chattering, a common problem with conventional SMC. In [9], an asymptotic SMC method is applied to both voltage and current controllers within a cascaded framework for GFMIs. Although [9] outlines principles for selecting control parameters for SMC, the selection principles employed in [7], [8], and [9] rely on trial-and-error, which may not guarantee optimal performance.

To address the aforementioned shortcomings, this paper introduces a novel PSO-FSMC method for voltage and current control within a cascaded framework for GFMIs. The principal contributions of this article are:

- This paper presents a new design of sliding surfaces and control laws for GFMIs aimed at reducing chattering, avoiding singularity issues, and ensuring both rapid dynamic responses and high robustness. The design process is thoroughly elaborated through detailed analytical stability analysis.
- An innovative approach is proposed using the PSO algorithm to optimize 24 control parameters of the proposed FSMC for GFMIs. This optimization specifically targets the reduction of tracking errors during the transition from off-grid to on-grid modes.
- Comparative evaluations are conducted against a well-established PI controller [1], commonly used in GFMI applications, during transitions from off-grid to grid-tied modes under two critical grid scenarios (ultra-weak and ultra-strong). The results demonstrate that the proposed PSO-FSMC significantly enhances the performance of both voltage and current controllers, achieving up to a 97% reduction in tracking errors compared to the PI controller.

II. Cascaded Voltage and Current Control Based on Novel PSO-FSMC

A. Model of a GFMI System

Fig. 1 depicts the investigated system featuring a three-phase GFMI supplying a local load (R) in off-grid operation through an LC filter. In this configuration, R_f and L_f represent the resistance and inductance of the LC filter inductor, respectively, while C_f is the capacitance of the LC filter capacitor. The three-phase voltages at the capacitor or point of common coupling (PCC) are denoted by v_oabc. Additionally, the utility grid is emulated by an AC voltage source (v_g), which is connected through an equivalent grid resistance (R_g) and inductance (L_g).

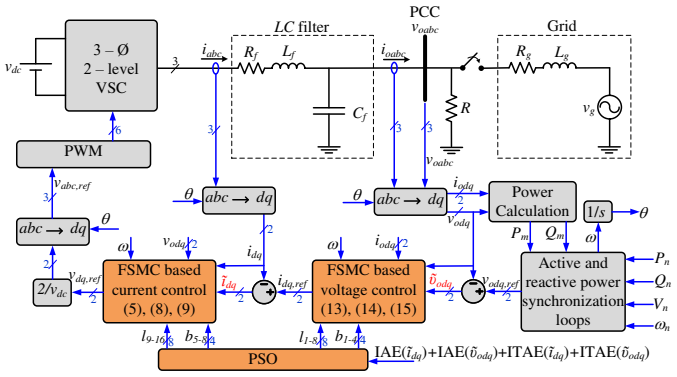

Fig. 1. Control structure of LC-filter-based GSMI.

As depicted in Fig. 1, the proposed control strategy includes power synchronization control (i.e., active and reactive power synchronization loops) and cascaded voltage and current control loops based on FSMC, with 24 control parameters optimized using PSO. For the power synchronization loops, droop controllers are utilized for both active and reactive power, as detailed in [1]. The cascaded voltage and current control loops, which are based on PSO-FSMC, will be elaborated on in subsequent sections.

For the GFMI system, the voltage balance equations across the LC filter inductor can be obtained in the dq reference frame as:

$$\begin{cases} \dot{i}_d = -\frac{R_\mathrm{f}}{L_\mathrm{f}} i_d + \frac{1}{L_\mathrm{f}} v_d - \frac{1}{L_\mathrm{f}} v_{od} + \omega i_q \\ \dot{i}_q = -\frac{R_\mathrm{f}}{L_\mathrm{f}} i_q + \frac{1}{L_\mathrm{f}} v_q - \frac{1}{L_\mathrm{f}} v_{oq} - \omega i_d. \end{cases} \tag{1}$$

Similarly, the current balance equations across the LC filter capacitor can be obtained in the dq reference frame as:

$$\begin{cases} \dot{v}_{od} = \frac{1}{C_\mathrm{f}} i_d - \frac{1}{C_\mathrm{f}} i_{od} + \omega v_{oq} \\ \dot{v}_{oq} = \frac{1}{C_\mathrm{f}} i_q - \frac{1}{C_\mathrm{f}} i_{oq} - \omega v_{od}. \end{cases} \tag{2}$$

B. Current Loop Control based on FSMC

The current controller is designed to accurately and quickly track the reference currents ($i_{dq,ref}$) provided by the voltage controller. To initiate the design process, let us first define the current tracking error in the dq reference frame:

$$\begin{cases} \tilde{i}_d = i_{d,ref} - i_d \\ \tilde{i}_q = i_{q,ref} - i_q. \end{cases} \tag{3}$$

where $\tilde{i}_d$ and $\tilde{i}_q$ are the current tracking errors, $i_{d,ref}$ and $i_{q,ref}$ are the reference currents provided by the voltage controller.

In general, the design of a SMC with fixed-time stability involves two key steps:

1) Designing a stable sliding surface that ensures the desired fixed-time behavior once the inverter dynamics are constrained to evolve along it; and

2) Developing a control law that drives the inverter dynamics to reach the designed sliding surface within a fixed timeframe.

To ensure that i_{dq} reaches $i_{dq,ref}$ within a fixed time during the sliding phase, the sliding surfaces are constructed as follows:

$$\begin{cases} s_{id} = \dot{\tilde{i}}_d + l_1|\tilde{i}_d|^{\frac{b_1}{b_2}} sgn\left(\tilde{i}_d\right) + l_2|\tilde{i}_d|^{\frac{b_3}{b_4}} sgn\left(\tilde{i}_d\right) \\ s_{iq} = \dot{\tilde{i}}_q + l_3|\tilde{i}_q|^{\frac{b_1}{b_2}} sgn\left(\tilde{i}_q\right) + l_4|\tilde{i}_q|^{\frac{b_3}{b_4}} sgn\left(\tilde{i}_q\right). \end{cases} \tag{4}$$

where $\dot{\tilde{i}}_d$ and $\dot{\tilde{i}}_q$ represent the time derivatives of the tracking errors, as defined in (3). The control parameters $l_1, l_2, l_3, l_4, b_1, b_2, b_3$, and b_4 must be selected within their respective constraints (as explained in Remark 1). Given that the controller's performance is highly sensitive to the selection of these parameters, PSO is employed to determine their optimal values and enhance overall system performance.

The design of the SMC control law is structured around two main components: the equivalent control function ($v_{dq,eq}$), which ensures reachability to the sliding surface, and the switching control function ($v_{dq,sw}$), which guarantees fixed-time stability and a high degree of robustness. The control law is:

$$v_{dq} = v_{dq,eq} + v_{dq,sw}. \tag{5}$$

When the sliding surface is reached, the motion along the sliding surface will maintain $[s_{id}, s_{iq}] = [0, 0]$ for $t > 0$. This principle aids in designing the equivalent control function. To begin with the design of the equivalent control function for the d-component ($v_{d,eq}$), let us first simplify the sliding surface:

$$\begin{aligned} s_{id} &= \dot{\tilde{i}}_d + l_1|\tilde{i}_d|^{\frac{b_1}{b_2}} sgn\left(\tilde{i}_d\right) + l_2|\tilde{i}_d|^{\frac{b_3}{b_4}} sgn\left(\tilde{i}_d\right) \xrightarrow{using\ (1)\ \&\ (3)} \\ &= \dot{i}_{d,ref} - \left(-\frac{R_\mathrm{f}}{L_\mathrm{f}} i_d + \frac{1}{L_\mathrm{f}} v_d - \frac{1}{L_\mathrm{f}} v_{od} + \omega i_q\right) \\ &\quad + l_1|\tilde{i}_d|^{\frac{b_1}{b_2}} sgn\left(\tilde{i}_d\right) + l_2|\tilde{i}_d|^{\frac{b_3}{b_4}} sgn\left(\tilde{i}_d\right). \end{aligned} \tag{6}$$

From (6), to drive s_{id} to zero, the equivalent control function ($v_{d,eq}$) must be designed as follows:

$$\begin{aligned} s_{id} = \dot{i}_{d,ref} - \Bigg(&- \frac{R_\mathrm{f}}{L_\mathrm{f}} i_d + \frac{1}{L_\mathrm{f}} \Bigg(L_\mathrm{f} \Bigg(+ \frac{R_\mathrm{f}}{L_\mathrm{f}} i_d + \frac{1}{L_\mathrm{f}} v_{od} - \omega i_q \\ &+ \dot{i}d, ref + l_1|\tilde{i}_d|^{\frac{b_1}{b_2}} sgn\left(\tilde{i}_d\right) + l_2|\tilde{i}_d|^{\frac{b_3}{b_4}} sgn\left(\tilde{i}_d\right) \Bigg) \Bigg) \\ &- \frac{1}{L_\mathrm{f}} v_{od} + \omega i_q \Bigg) \\ &+ l_1|\tilde{i}_d|^{\frac{b_1}{b_2}} sgn\left(\tilde{i}_d\right) + l_2|\tilde{i}_d|^{\frac{b_3}{b_4}} sgn\left(\tilde{i}_d\right) = 0. \end{aligned} \tag{7}$$

Similarly, the equivalent control function for the q-component ($v_{q,eq}$) can be designed. Thus, the equivalent control functions for both the d- and q-components are derived as follows:

$$\begin{cases} v_{d,eq} = L_\mathrm{f} \Bigg(+ \frac{R_\mathrm{f}}{L_\mathrm{f}} i_d + \frac{1}{L_\mathrm{f}} v_{od} - \omega i_q \\ \qquad + \dot{i}d, ref + l_1|\tilde{i}_d|^{\frac{b_1}{b_2}} sgn\left(\tilde{i}_d\right) + l_2|\tilde{i}_d|^{\frac{b_3}{b_4}} sgn\left(\tilde{i}_d\right) \Bigg) \\ v_{q,eq} = L_\mathrm{f} \Bigg(+ \frac{R_\mathrm{f}}{L_\mathrm{f}} i_q + \frac{1}{L_\mathrm{f}} v_{oq} + \omega i_d \\ \qquad + \dot{i}q, ref + l_3|\tilde{i}_q|^{\frac{b_1}{b_2}} sgn\left(\tilde{i}_q\right) + l_4|\tilde{i}_q|^{\frac{b_3}{b_4}} sgn\left(\tilde{i}_q\right) \Bigg). \end{cases} \tag{8}$$

To ensure rapid dynamic response within a fixed timeframe and to guarantee a high degree of robustness, the switching control function is constructed as follows:

$$\begin{cases} \dot{v}_{d,sw} = L_\mathrm{f} \Big(l_5|s_{id}|^{\frac{b_1}{b_2}} sgn\left(s_{id}\right) + l_6|s_{id}|^{\frac{b_3}{b_4}} sgn\left(s_{id}\right) \Big) \\ \dot{v}_{q,sw} = L_\mathrm{f} \Big(l_7|s_{iq}|^{\frac{b_1}{b_2}} sgn\left(s_{iq}\right) + l_8|s_{iq}|^{\frac{b_3}{b_4}} sgn\left(s_{iq}\right) \Big). \end{cases} \tag{9}$$

Here, $\dot{v}d, sw$ and $\dot{v}q, sw$ are the time derivatives of the switching control functions, and $l_5, l_6, l_7, l_8, b_1, b_2, b_3$, and b_4 are control parameters that must be selected within their respective constraints to ensure system stability (as outlined in Remark 1). PSO is employed to optimize these parameters, thereby enhancing the overall controller performance.

The proof of fixed-time stability for the closed-loop system, utilizing the FSMC-based current controller, is derived by employing methods analogous to those used in [10], leveraging the principles of Lyapunov stability theory. For this purpose, the following candidate Lyapunov function is defined:

$$V = \frac{1}{2} s_{id}^2 + \frac{1}{2} s_{iq}^2. \tag{10}$$

C. Voltage Loop Control based on FSMC

The voltage controller is designed to enable the GFMI system to follow the reference voltage generated by the power control loop ($v_{odq,ref}$). To achieve this, let us first define the voltage tracking error in the dq reference frame:

$$\begin{cases} \tilde{v}_{od} = v_{od,ref} - v_{od} \\ \tilde{v}_{oq} = v_{oq,ref} - v_{oq}. \end{cases} \tag{11}$$

where $\tilde{v}_{od}$ and $\tilde{v}_{oq}$ are the voltage tracking errors, $v_{od,ref}$ and $v_{oq,ref}$ are the reference voltages provided by the power control loop.

To ensure that v_{odq} reaches $v_{odq,ref}$ within a fixed timeframe during the sliding phase, the sliding surfaces are designed as follows:

$$\begin{cases} s_{vod} = \dot{\tilde{v}}_{od} + l_9|\tilde{v}_{od}|^{\frac{b_5}{b_6}} sgn\left(\tilde{v}_{od}\right) + l_{10}|\tilde{v}_{od}|^{\frac{b_7}{b_8}} sgn\left(\tilde{v}_{od}\right) \\ s_{voq} = \dot{\tilde{v}}_{oq} + l_{11}|\tilde{v}_{oq}|^{\frac{b_5}{b_6}} sgn\left(\tilde{v}_{oq}\right) + l_{12}|\tilde{v}_{oq}|^{\frac{b_7}{b_8}} sgn\left(\tilde{v}_{oq}\right). \end{cases} \tag{12}$$

Here, $\dot{\tilde{v}}_{od}$ and $\dot{\tilde{v}}_{oq}$ are the time derivatives of the tracking errors (as defined in (11)), and $l_9, l_{10}, l_{11}, l_{12}, b_5, b_6, b_7$, and b_8 are control parameters that must be selected within their respective constraints to ensure the stability of the closed-loop system (as elaborated in Remark 1). Since the controller

performance is highly sensitive to the selection of these parameters, PSO is proposed to optimize their values and enhance overall controller performance.

When the sliding surface is reached, the motion along the sliding surface will maintain $[s_{id}, s_{iq}] = [0, 0]$ for $t > 0$. Accordingly, following the logic used in the derivation of the equivalent current control (as given by (6) and (7)), the equivalent control function can be derived as:

$$\begin{cases} i_{d,eq} = C_{\mathrm{f}}\Big(+ \dfrac{1}{C_{\mathrm{f}}} i_{od} - \omega v_{oq} + \dot{v}_{od,ref} \\ \qquad + l_9 |\tilde{v}_{od}|^{\frac{b_5}{b_6}} sgn\left(\tilde{v}_{od}\right) + l_{10} |\tilde{v}_{od}|^{\frac{b_7}{b_8}} sgn\left(\tilde{v}_{od}\right) \Big) \\ i_{q,eq} = C_{\mathrm{f}}\Big(+ \dfrac{1}{C_{\mathrm{f}}} i_{oq} + \omega v_{od} + \dot{v}_{oq,ref} \\ \qquad + l_{11} |\tilde{v}_{oq}|^{\frac{b_5}{b_6}} sgn\left(\tilde{v}_{oq}\right) + l_{12} |\tilde{v}_{oq}|^{\frac{b_7}{b_8}} sgn\left(\tilde{v}_{oq}\right) \Big). \end{cases} \tag{13}$$

To ensure robustness and a rapid dynamic response within a fixed timeframe for the voltage controller, an additional control function is designed and integrated with the equivalent control function ($i_{dq,eq}$) to generate the current reference as:

$$i_{dq,ref} = i_{dq,eq} + i_{dq,sw}. \tag{14}$$

The switching function is constructed as follows:

$$\begin{cases} \dot{i}_{d,sw} = C_{\mathrm{f}}\Big(l_{13} |s_{id}|^{\frac{b_1}{b_2}} sgn\left(s_{id}\right) + l_{14} |s_{id}|^{\frac{b_3}{b_4}} sgn\left(s_{id}\right) \Big) \\ \dot{i}_{q,sw} = C_{\mathrm{f}}\Big(l_{15} |s_{iq}|^{\frac{b_1}{b_2}} sgn\left(s_{iq}\right) + l_{16} |s_{iq}|^{\frac{b_3}{b_4}} sgn\left(s_{iq}\right) \Big). \end{cases} \tag{15}$$

Here, $\dot{i}_{d,sw}$ and $\dot{i}_{q,sw}$ are the time derivatives of the switching control functions, and the control parameters $l_{13}, l_{14}, l_{15}, l_{16}, b_1, b_2, b_3$, and b_4 must be selected in accordance with their respective constraints (as explained in Remark 1). Since the controller's performance can be significantly affected by these parameters, PSO is employed to optimize their values, thereby enhancing the overall system performance.

The proof of fixed-time stability for the closed-loop system, utilizing the FSMC-based voltage controller, is derived by employing the candidate Lyapunov function (10), following the approach outlined in [10].

Remark 1: Based on Lyapunov stability analysis, the control parameters for the voltage and current controllers must adhere to the following constraints to achieve fixed-time stability: l_1 through l_{16} and b_1 through b_4 must be positive constants. Additionally, the ratios must satisfy $0 < \frac{b_1}{b_2} < 1$, and $\frac{b_3}{b_4} > 1$.

D. Proposed PSO-FSMC

FSMC involves numerous control parameters that are often determined through trial-and-error. However, this approach is generally impractical and unlikely to yield a sensible solution. Therefore, an optimization-based strategy is a more logical and systematic alternative. Given the critical impact of these parameters on the controller's performance, this paper proposes an optimized FSMC framework that employs PSO to tune the control parameters. The primary objective is to minimize tracking errors, evaluated using the Integral of Absolute Error (IAE) and the Integral of Time-weighted Absolute Error (ITAE) performance indices.

Algorithm 1: PSO-based optimization framework for FSMC

1. **Initialize:**
   Set $t \leftarrow 0$
   Set SwarmSize $\leftarrow 20$
   Randomly initialize each particle's position $X_i(0)$ within predefined bounds, aligning with limits set in MATLAB for each of the 24 control parameters (l_1 to l_{16} and b_1 to b_8).
2. **While Termination Criteria not met:**
   a. **Evaluate the Swarm:**
      For each particle i in SwarmSize:
         Calculate $F(\text{IAE}, \text{ITAE})$ using MATLAB/Simulink model.
   b. **Update Personal and Global Bests:**
      For each particle i:
         If $F(\text{IAE}, \text{ITAE})_i < F(\text{IAE}, \text{ITAE})_{\text{pbest}_i}$:
            Update $\text{pbest}_i \leftarrow X_i$.
         If $F(\text{IAE}, \text{ITAE})_i < F(\text{IAE}, \text{ITAE})_{\text{gbest}}$:
            Update gbest $\leftarrow X_i$.
   c. **Update Velocity and Position:**
      For each particle i:
         Update velocity: $V_i(t+1) = w \cdot V_i(t) + c_1 \cdot \text{rand}() \cdot (\text{pbest}_i - X_i(t)) + c_2 \cdot \text{rand}() \cdot (\text{gbest} - X_i(t))$, where $c_1 = 1.49$, $c_1 = 1.49$, $w = [0.1; 1.1]$.
         Update position: $X_i(t+1) = X_i(t) + V_i(t+1)$.
   d. **Check for Termination:**
      Increment t.
      If $t \geq$ MaxIterations=10, terminate the loop
3. **Output:**
   Apply the best set of parameters from gbest to configure the FSMC in the Simulink model.
   Perform further validation and performance assessment.

1) Algorithm Implementation using PSO: PSO is a robust metaheuristic algorithm inspired by the social behaviors of biological species, extensively applied across various optimization contexts [11]. In this research, PSO is utilized to precisely adjust 24 control parameters of the FSMC, which include l_1 through l_{16} and b_1 through b_8. Within the PSO framework, these parameters are conceptualized as particles. The objective is to systematically refine their settings to minimize the cost function $F(IAE, ITAE)$, which quantitatively evaluates the tracking performance of the control system:

$$\begin{aligned} F(IAE, ITAE) = IAE(\tilde{i}_d) + ITAE(\tilde{i}_q) \\ + IAE(\tilde{v}_{od}) + ITAE(\tilde{v}_{oq}). \end{aligned} \tag{16}$$

where $IAE(\tilde{i}_{dq}) = \int_0^{t_{\mathrm{f}}} |\tilde{i}_{dq}|\, dt$ and $ITAE(\tilde{v}_{odq}) = \int_0^{t_{\mathrm{f}}} t|\tilde{v}_{odq}|\, dt$. Here, t_{f} denotes the total evaluation period. These metrics, IAE and ITAE, respectively measure the aggregate magnitude of error and the urgency of error correction over time, offering insights into the controller's accuracy and effectiveness in ensuring system stability and performance.

2) Algorithm Description: The PSO-based optimization framework, outlined in Algorithm 1, systematically refines FSMC control settings through iterative adjustments based on performance feedback from simulations.

III. Simulation Results

The proposed control method is evaluated and compared with a well-established PI controller [1] through a sim-

TABLE I
PARAMETERS OF THE GFMI SYSTEM, PI CONTROLLER, AND POWER SYNCHRONIZATION CONTROL

Plant Parameter	**Value**	**Control Parameter**	**Value**
L_{f}	10 mH	$k_{\mathrm{p_v}}$	0.5
R_{f}	0.1 Ω	$k_{\mathrm{i_v}}$	400
C_{f}	50 μF	$k_{\mathrm{p_c}}$	31.4159
P_{n}	1 p.u	$k_{\mathrm{i_c}}$	314.159
Q_{n}	0 p.u	α_{p}	0.0005
v_{g}	1 p.u	α_{q}	0.0001
ω_{n}	100π rad/s	τ_{p}	0.031415 s
-	-	τ_{q}	0.031415 s
Base VA Rating	**Value**	**Base V Rating**	**Value**
S_{n}	20 kVA	V_{n}	326.6 V

ulation of a GFMI, as depicted in Fig. 1, using MATLAB/SimPowerSystems. The parameters for the GFMI system, provided in Table I, are selected based on practical high power and current ratings typical in real-life applications. The parameters for the PI controllers, adopted from [1], are also detailed in Table I.

To ensure a fair comparison and concentrate on the performance of the capacitor voltage and inverter current controllers, this paper employs the same active and reactive power synchronization loops using the droop controllers from [1]. The control parameters of the proposed FSMC were optimized using the PSO described in Algorithm 1, with the optimized parameters detailed in Table II. To determine the limits for the PSO-optimized FSMC control parameters, they must first be selected within their respective constraints to ensure the stability of the closed-loop system (as explained in Remark 1). In addition to stability, these parameters are chosen to meet critical design specifications such as chattering reduction, robust performance, and fast dynamic response with minimal transient overshoot. Specifically, the parameters l_1–l_4 and l_9–l_{12} correspond to the sliding surfaces, while l_5–l_8 and l_{13}–l_{14} are associated with the switching control laws. To achieve the desired performance, the sliding surface parameters are assigned relatively larger values than those used in the switching control laws, which helps minimize chattering, ensure a fast dynamic response during the sliding phase, and improve robustness. Additionally, the parameters b_1–b_8 are selected to satisfy the conditions $0 < \frac{b_1}{b_2} < 1$ and $\frac{b_3}{b_4} > 1$ (as detailed in Remark 1), with both ratios ($\frac{b_1}{b_2}$ and $\frac{b_3}{b_4}$) chosen close to unity. This parameter selection strategy reduces transient overshoot and enhances convergence speed. Further details on these design principles can be found in [10].

The simulation study primarily assesses the performance of the proposed controller during the transition from off-grid to grid-tied mode. The tests are conducted under two critical grid scenarios: an ultra-weak grid condition ($SCR = 1$) and an ultra-strong grid condition ($SCR = 30$). The GFMI is initially operated in islanded mode and subsequently connected to the grid at $t = 0.1$ s. The impedance values of the grid are adjusted to maintain a constant X/R ratio of 5 in both grid scenarios.

Figs. 2(a)–2(d) compare the tracking performance of the proposed PSO-FSMC and the PI controller for both voltage and current control loops during the transition from off-grid to grid-tied operation under an ultra-weak grid scenario ($SCR = 1$). While both controllers exhibit minimal deviation at the transition point ($t = 0.1, \mathrm{s}$), the PSO-FSMC consistently outperforms the PI controller, demonstrating reduced overshoot, faster dynamic response, and significantly lower tracking errors in both transient and steady-state conditions.

Figs. 3(a)–3(d) compare the tracking performance of voltage and current controllers using the proposed PSO-FSMC and the PI controller during the transition from autonomous to grid-connected operation under an ultra-strong grid condition ($SCR = 30$). The PI controller shows significant transient overshoots in both voltage and current responses. In contrast, the PSO-FSMC effectively mitigates these overshoots, delivering a faster dynamic response and rapid convergence to the reference values. These results highlight the robustness and superior performance of the proposed controller under extreme

TABLE II
CONTROL PARAMETERS OF FSMC OPTIMIZED BY PSO FOR TWO DIFFERENT GRID CONDITIONS

Gain	**Value** ($SCR = 1$)	**Value** ($SCR = 30$)	**Range**
l_1	10000	4.3616×10^3	[1000, 10000]
l_2	3.5992×10^3	9.3503×10^3	[1000, 10000]
l_3	7.8185×10^3	5.3463×10^3	[1000, 10000]
l_4	10000	5.7126×10^3	[1000, 10000]
l_5	2000	2000	[500, 2000]
l_6	2000	1.9950×10^3	[500, 2000]
l_7	500	1.3977×10^3	[500, 2000]
l_8	2000	500	[500, 2000]
l_9	9.9688×10^3	9.9875×10^3	[1000, 10000]
l_{10}	9.9585×10^3	10000	[1000, 10000]
l_{11}	10000	7.1891×10^3	[1000, 10000]
l_{12}	7.4362×10^3	3.4463×10^3	[1000, 10000]
l_{13}	2000	2000	[500, 2000]
l_{14}	2000	2000	[500, 2000]
l_{15}	688.2809	1.9988×10^3	[500, 2000]
l_{16}	522.8598	1.9190×10^3	[500, 2000]
b_1	1.0007×10^3	999.4927	[990, 1001]
b_2	1013	1.0028×10^3	[1002, 1013]
b_3	1013	1.0073×10^3	[1002, 1013]
b_4	990	998.8802	[990, 1001]
b_5	1.0004×10^3	1001	[990, 1001]
b_6	1002	1002	[1002, 1013]
b_7	1013	1.0109×10^3	[1002, 1013]
b_8	990	990	[990, 1001]

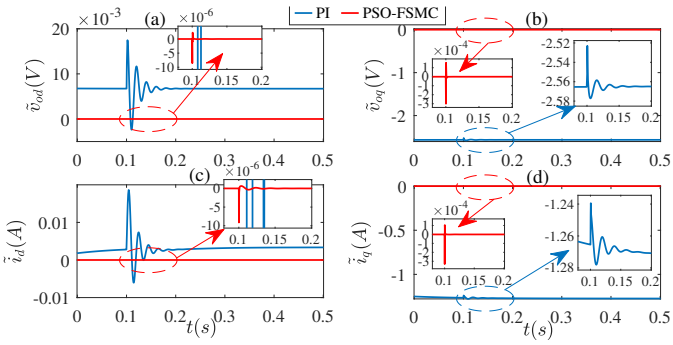

Fig. 2. Comparison of voltage and current tracking errors using PSO-FSMC and PI controllers for $SCR = 1$.

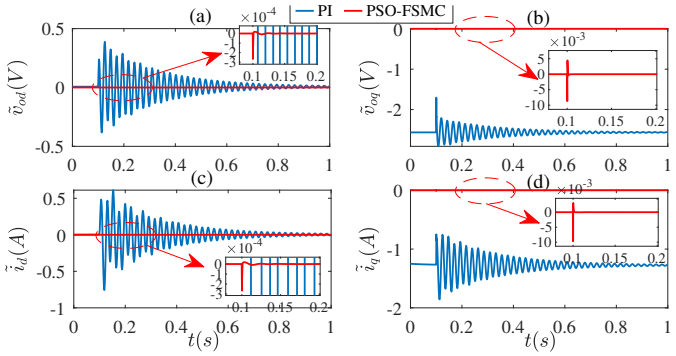

Fig. 3. Comparison of voltage and current tracking errors using PSO-FSMC and PI controllers for $SCR = 30$.

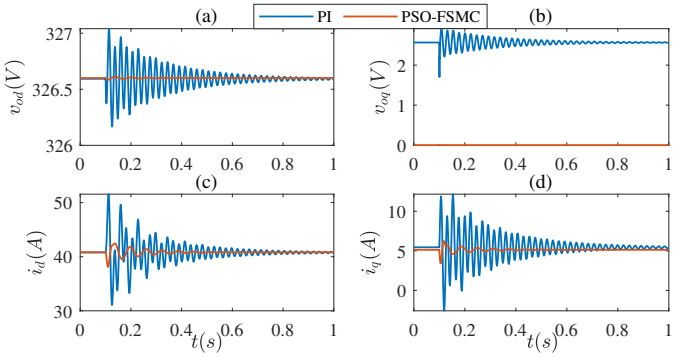

Fig. 4. Output voltage and filter current controlled by PSO-FSMC and PI for $SCR = 30$: (a) v_{od}, (b) v_{oq}, (c) i_d, (d) i_q.

grid conditions.

In Fig. 4, the performance of the proposed PSO-FSMC method is evaluated against a PI controller by comparing the controlled output voltage at the PCC and the filter current in the dq reference frame. This assessment occurs during the transition from autonomous to grid-connected modes within an ultra-strong grid scenario ($SCR = 30$). Significant deviations are observed in the transient response from off-grid to on-grid when using the PI controller, potentially risking damage to inverter switches due to high inrush currents caused by notable voltage fluctuations. As illustrated in Fig. 4, the PSO-FSMC method effectively mitigates these variations, demonstrating a substantial reduction in transient deviations and enhancing the system's stability.

Table III provides a quantitative comparison between the proposed PSO-FSMC and the PI controller under both ultra-weak ($SCR = 1$) and ultra-strong ($SCR = 30$) grid conditions. The comparison utilizes the combined IAE and ITAE, $F(IAE, ITAE)$, as defined in (16) with $t_f = 1s$. The results demonstrate that the PSO-FSMC achieves approximately a 97% improvement in both grid scenarios compared to the PI controller, highlighting significant performance enhancements. These results also highlight the limitations of conventional PI control under extreme grid conditions, underscoring the importance of advanced control strategies such as PSO-FSMC in ensuring robust and efficient performance.

TABLE III
NUMERICAL COMPARISON OF THE CONTROLLERS

Grid Conditions	Ultra Weak Grid		Ultra Strong Grid	
Criteria	PI	PSO-FSMC	PI	PSO-FSMC
$F(IAE, ITAE)$	5.8702	0.1509	6.0731	0.1525

IV. CONCLUSION

Ensuring a seamless transition from autonomous to grid-tied modes for GFMI systems presents a critical challenge. This paper proposes an effective solution through the development of a novel and straightforward design of FSMC. The proposed method is applied to both capacitor voltage and current controllers within a cascaded framework for GFMIs. A key challenge in implementing advanced sliding mode controllers such as FSMC lies in selecting control parameters to achieve optimal performance—a task that is generally unfeasible through manual tuning. To overcome this, 24 FSMC parameters are systematically optimized using PSO. Comparative simulation evaluations of the transition from off-grid to on-grid mode under different grid conditions demonstrate that PSO-FSMC provides a robust solution, enabling a seamless transition with no chattering and a rapid response, significantly outperforming a well-established PI controller. The proposed method significantly reduces tracking errors, as confirmed by a 97% improvement in tracking performance compared to the PI controller.

REFERENCES

[1] A. Pal, D. Pal, and B. K. Panigrahi, "A current saturation strategy for enhancing the low voltage ride-through capability of grid-forming inverters," IEEE Transactions on Circuits and Systems II: Express Briefs, vol. 70, no. 3, pp. 1009-1013, 2022.

[2] D. B. Rathnayake et al., "Grid forming inverter modeling, control, and applications," IEEE Access, vol. 9, pp. 114781-114807, 2021.

[3] A. Alassi, Z. Feng, K. Ahmed, M. Syed, A. Egea-Alvarez, and C. Foote, "Grid-forming VSM control for black-start applications with experimental PHiL validation," International Journal of Electrical Power & Energy Systems, vol. 151, p. 109119, 2023.

[4] J. Alonso-Mart´ınez, J. E. G. Carrasco, and S.Arnaltes, "Table-based direct power control: A critical review for microgrid applications," IEEE Trans. Power Electron., vol. 25, no. 12, pp. 2949–2961, Dec. 2010.

[5] Y. Luo, C. Liu, and F. Yu, "Predictive current control of a new three-phase voltage source inverter with phase shift compensation," IET Electric Power Applications, vol. 11, no. 5, pp. 740–748, 2017.

[6] D. Chen, J. Zhang, and Z. Qian, "An improved repetitive control scheme for grid-connected inverter with frequency-adaptive capability," IEEE Trans. Ind. Electron., vol. 60, no. 2, pp. 814–823, Feb. 2013.

[7] T. S. Das, U. D. Annakkage, D. Muthumuni, and I. K. Park, "Robust higher order sliding mode control of grid-forming converters with LCL filter in weak grid scenarios for fast frequency support," IET Generation, Transmission & Distribution, vol. 18, no. 23, pp. 3851-3862, 2024.

[8] Z. Li, C. Zang, P. Zeng, H. Yu, S. Li, and J. Bian, "Control of a grid-forming inverter based on sliding-mode and mixed H_2/H_∞ control," IEEE Transactions on Industrial Electronics, vol. 64, no. 5, pp. 3862-3872, 2016.

[9] Z. Li et al., "Virtual synchronous generator and SMC-based cascaded control for voltage-source grid-supporting inverters," IEEE J. Emerg. Sel. Topics Power Electron., vol. 10, no. 3, pp. 2722–2736, Jun. 2022.

[10] P. A. Hosseinabadi, S. Mekhilef, H. Pota, and M. Kermadi, "Chattering free Fixed-time robust sliding mode controller for grid-connected inverters under parameter variations," IEEE Journal of Emerging and Selected Topics in Power Electronics, vol. 12, no. 1, pp. 579-592, 2024.

[11] M. Negnevitsky, Artificial intelligence: a guide to intelligent systems. Pearson education, 2005.